便携式电火花沉积镍基合金工艺

张 平[1]，马 琳[1,2]，梁志杰[1]，张二亮[1]
（1. 装甲兵工程学院 再制造重点实验室，北京 100072；
2. 防化指挥工程学院 履约事务办公室，北京 102205）

张 平

摘 要：通过便携式电火花表面强化设备在 45钢表面制备镍基合金强化层，从沉积层厚度、沉积层硬度和沉积层微观缺陷三个方面分析了各工艺参数对强化层质量的影响。通过试验分析确定采用该便携设备进行沉积修复时，选用输出功率为 1.2 kW，输出电压为 128 V，保护气流量为 5 L/min的工艺时可获得综合质量最优的沉积层，并在此工艺参数条件下制备了厚为 595 μm，硬度高达 362 HV，无明显缺陷镍基合金沉积层。
关键词：电火花表面强化；镍基合金；沉积工艺
中图分类号：TG115.28　文献标识码：A　文章编号：0253－360X(2011)04－0033－04

0 序　言

电火花表面强化技术可以获得质量良好的沉积层，其优越的可操作性和现场修复能力使其在工业中尤其在模具修复上具有其他工艺所不及的优点[1－4]. 以镍基合金为电极采用电火花表面强化技术在工具钢基体上制备强化层可以使工件的表面性能得到明显提高. 现场修复中，便携式电火花设备应用最为广泛. 文中主要对镍基合金沉积层的性能进行研究，旨在优化电火花沉积工艺，为该技术的实际应用奠定基础.

1 试验方法

电火花表面强化修复技术把待沉积材料作为工作电极（阳极），在氩气保护下使之与金属基体（阴极）之间产生火花放电，在 10^{-5} ~10^{-6} s时间内电极与工件接触的部位达到 8 000 ~25 000 ℃的高温，利用火花放电的能量，将电极材料转移至工作表面，构成沉积层的沉积方法. 这一过程大致可以分为以下 4个阶段[5]：（1）电容充电，电极向工件运动（图 1a）；（2）空气间隙被击穿，产生电火花放电，电极与工件材料局部熔化甚至汽化（图 1b）；（3）电极与工件接触，停止放电，接触点流过短路电流，继续加热. 电极继续下降以适当压力压向工件，使熔化的材料相互粘接或扩散，形成或产生化合物熔渗层（图 1c）；（4）电极离开工件，放电部位急剧冷却（图 1d）.

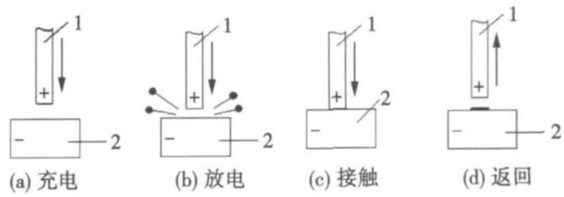

图 1　电火花表面强化技术的原理过程示意图
Fig. 1　Program of electric-sparkle deposition

试验以工业上常用的 45钢为基体，直径为 2.4 mm的镍基合金 NICR398为电极进行试验. 电极化学成分如表 1所示. 试验选用设备为便携式金属表面强化冷补机，主要工艺参数包括输出功率、输出电压、保护气流，按表 2调整参数进行电火花表面强化试验.

表 1　电极材料主要成分及含量（质量分数，%）
Table 1　Chemical compositions of electrode

Nb	Cr	Mn	Fe	Co	Ni
1.14	16.17	2.80	2.02	0.29	77.58

试验沉积面积为 1 cm²，沉积时间为 30 min. 沉积前后分别采用精度为 0.000 1 g的分析天平对沉积层增重和电极失重进行测量. 采用奥林巴斯金相显微镜测量沉积层厚度，采用维式硬度测量仪测量沉积层硬度值，采用扫描电镜对沉积层与基体交

收稿日期：2010－04－07

界处的组织结构进行分析.

表 2 试验编号与工艺参数

Table 2 Number of technology parameters

编号	输出电压 U/V	输出功率 P/kW	保护气流量 q/(L·min⁻¹)	基体增重 Δg_1/g	电极减重 Δg_2/g
1	130	0.9	0	0.118 0	0.193 1
2	130	0.9	3	0.047 9	0.121 3
3	130	0.9	5	0.085 2	0.130 7
4	130	0.9	7	0.058 3	0.066 5
5	98	0.9	5	0.016 4	0.024 8
6	144	0.9	5	0.107 6	0.153 9
7	177	0.9	5	0.235 9	0.256 2
8	130	0.6	5	0.035 7	0.050 5
9	130	1.2	5	0.090 7	0.133 4
10	130	1.5	5	0.113 6	0.154 9

2 试验结果与分析

2.1 沉积工艺对沉积层厚度和质量的影响

图 2分别表示的是保护气流量、输出电压和输出功率对沉积层厚度的影响.

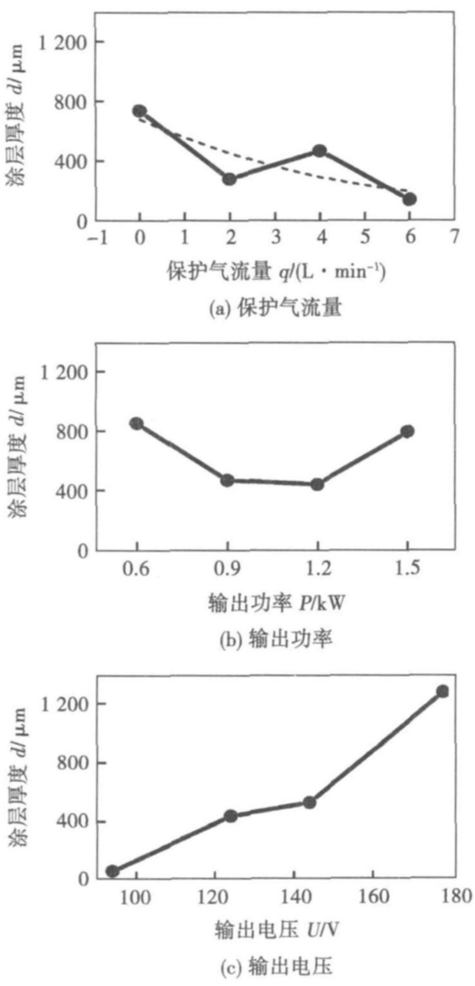

图 2 工艺参数对电火花堆焊沉积层厚度影响

Fig. 2 Influence of processing parameters on thickness

对保护气流量与强化层的厚度曲线进行拟合(图 2a),认为保护气流量对强化层厚度的影响呈单向反方向变化.保护气流量越大,冷却和吹动作用越强,使得熔融态电极材料迅速冷却呈固态后被迅速吹离,故此形成的强化层越薄.

输出功率对强化层厚度的影响呈双向变化(图 2b),图中可以看出当随着输出功率的增加强化层厚度降低及当输出功率达到一定值时(约为 1 kW),再次增大输出功率强化层厚度开始增大.输出功率直接影响电火花表面强化过程的热输入.当输出功率较低时,电极材料得不到充分熔化,致使强化层结合不紧密,孔隙较多,单位质量下的体积增大,即强化层厚度增加.同样,当输出功率过大时,电极材料熔化的体积增大,从一定程度上提高沉积效率,强化层厚度有所提高.

输出电压对强化层厚度的影响呈正向变化(图 2c)即输出电压越大,单位时间内获得的强化层厚度越大.电压越大,得到的电弧能量越大,故此可直接促进电极材料的熔化成形,提高沉积效率.电压越小,电弧能量就越小,电极材料熔化少,因此沉积层厚度小.图 2中可以看到,输出电压对强化层厚度的影响最为明显,输出功率次之,保护气流量最小.

2.2 沉积工艺对沉积层硬度的影响

利用显微硬度计对熔覆层的显微硬度进行测量,测量时选取载荷为 196 N,加载时间为 15 s,在覆层任意取 3点测量,取其平均值作为该覆层的显微硬度.

图 3分别表示了不同输出功率、输出电压及保护气流对沉积层显微硬度的影响.从图 3a中可以看出,随着保护气流的增大,沉积层的显微硬度随之提高.尤其是当保护气流量超过 3 L/min时,显微硬度的提高幅度明显增大.保护气流量的增大可以防止沉积过程中沉积层表面的氧化作用,从而起到提高沉积质量的作用.

输出功率越大,沉积层显微硬度也随之增大(图 3b).输出功率大表明焊接过程中的热输入大,电极材料的熔化更加充分,结合越致密,从而涂层硬度得到提高.但熔化材料结合能力有限,因此功率对强化层显微硬度的影响幅度很小.

图 3c表明随着输出电压的加大,沉积层的显微硬度减小.输出电压加大导致放电空间的能量提高,会对沉积层产生热影响,导致硬度降低.从图 3中得知,提高沉积层硬度,保护气流量最为重要,输出电压和输出功率的影响要小于保护气流量.

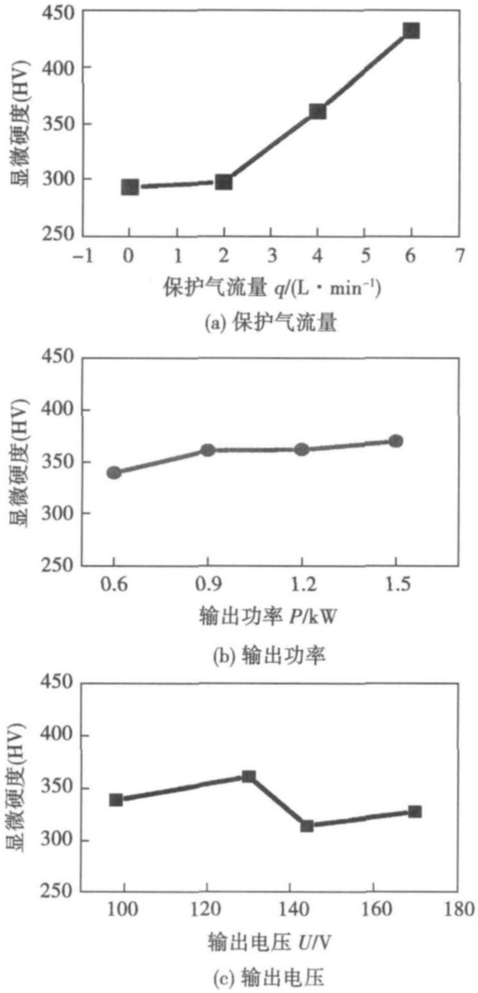

图 3　工艺参数对沉积层显微硬度的影响

Fig. 3　Influence of parameters on microhardness

2.3　沉积工艺对沉积层内微观缺陷的影响

图 4~图 6分别为金相显微镜下放大 500倍时沉积层的截面图. 在没有保护气流进行焊接的试验过程中, 刚刚成形的沉积层很快被氧化形成乌黑表面, 同时由于缺少吹动力, 部分熔化不充分和新凝固的电极颗粒其表面被氧化后不能及时排除, 被粘连在沉积层表面参与下一次沉积, 导致了沉积层间的结合不紧密, 出现气孔和氧化物杂质. 从图 4中可以看到, 当无保护气或是保护气流量较小时, 沉积层内空隙和微裂纹明显, 尤其是无保护气时, 孔隙与微裂纹已经出现相互交接的现象. 同时, 图 4还表明当保护气流增大到一定程度时, 保护气流的再增加对沉积层质量的改善已不明显. 当气体流量增加到 7 L/min时, 由于保护气的吹动作用加大, 影响了电极材料的堆积成形, 沉积内反而出现了微观孔隙和缺陷.

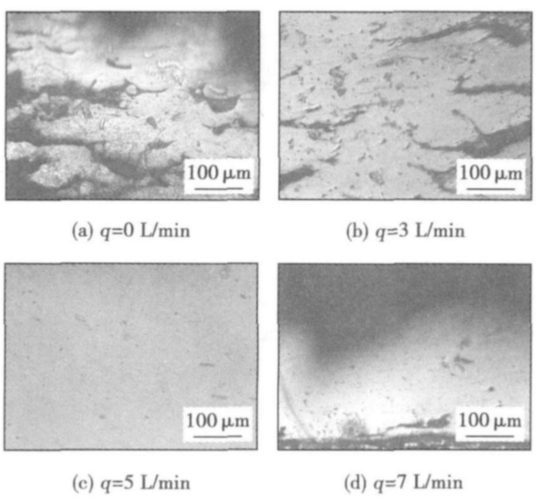

图 4　不同保护气流量下沉积层截面形貌

Fig. 4　Microstructure of cross_section of coating with different shielding gas flow

图 5中当输出功率为 0.9 kW时, 沉积层的质量最好, 1.2 kW时次之. 输出功率为 0.6 kW时, 电极材料熔化不充分, 相互堆垛到一起, 形成微观缺陷. 当功率为 1.5 kW时, 电极材料过热, 材料流动速率低于冷却速率, 同样会形成微观缺陷.

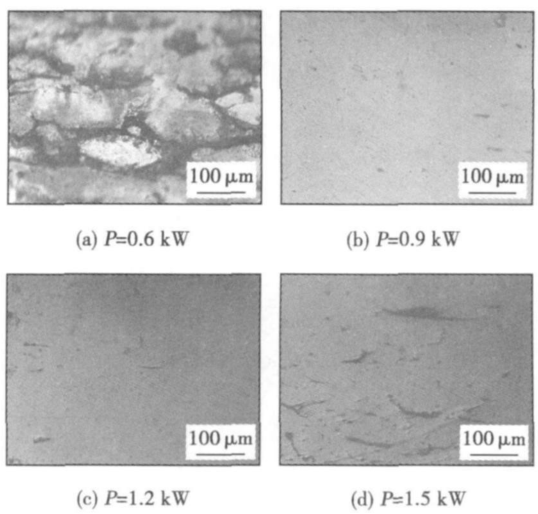

图 5　不同输出功率条件下沉积层截面形貌

Fig. 5　Microstructure of cross_section of coating with different output power

图 6所示输出电压越小, 沉积质量越好. 相同工艺条件下, 输出电压小, 可以有效避免沉积层的过热, 提高沉积质量.

3　镍基合金的工艺优化

在进行电火花修补的过程中, 不能单纯以提高沉积层硬度为目标. 应该在提高沉积层硬度的同时尽可能提高沉积效率 (即相同时间的沉积厚度)并

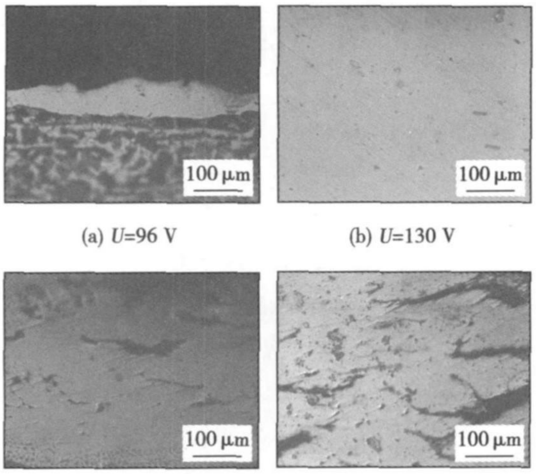

(a) U=96 V (b) U=130 V

(c) U=144 V (d) U=177 V

图 6 不同输出电压条件下沉积层截面示意图
Fig. 6 Microstructure of cross_section of coating with different output voltage

减少微观缺陷(微裂纹和孔隙)的产生. 为此, 对各个工艺参数对沉积层厚度、硬度和结合性的影响进行分析, 最后确定输出功率为 1.2 kW, 输出电压为 128 V, 保护气流量为 5 L/min 的工艺参数为获得镍基合金覆层的最佳工艺参数. 该工艺条件下横截面形貌如图 7 所示.

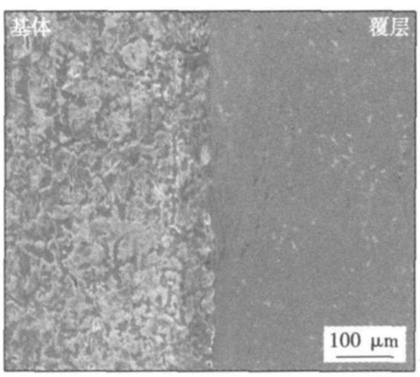

图 7 工艺优化后的截面形貌
Fig. 7 Microstructure of cross_section of coating

图 7 表明基体与沉积层交界处, 晶粒明显细化, 沉积层截面组织细密均匀无明显微观缺陷. 该沉积层厚为 595 μm, 平均显微硬度 362 HV, 约是 45 钢基体的 2 倍 (45 钢基体的显微硬度在同样测量条件下约为 178~182 HV).

4 结 论

(1) 输出电压对强化层厚度的影响最为明显, 电压越大, 强化层厚度越大. 输出功率的影响次之, 增大输出功率会降低沉积效率, 当输出功率提高到一定值时, 再增加功率时沉积层厚度有所提高, 其变化曲线为双向. 保护气流对沉积层厚度影响最小, 保护气流量越大, 厚度越低.

(2) 保护气流越大, 沉积层硬度越大; 在其它工艺参数不变的情况下, 沉积层的显微硬度随输出功率的增大而增大, 随着输出电压的增大而减小.

(3) 保护气流量与输出功率对沉积层结合质量的影响呈双向变化, 当流量和功率达到一定值时, 沉积层结合最紧密, 无明显孔洞缺陷; 当流量和功率大小向两边移动时, 沉积层缺陷增加. 同时输出电压越小, 得到的沉积层质量越好.

(4) 输出功率为 1.2 kW, 输出电压为 128 V, 保护气流量为 5 L/min 时可获得无明显缺陷镍基合金沉积层. 该沉积层厚度为 595 μm, 显微硬度 362 HV, 约是 45 钢基体的 2 倍.

参考文献:

[1] Galinov I V, Luban Mass R B. Transfer trends during electrospark alloying[J]. Surface and Coating Technology, 1996, 79(1-3): 9-18.

[2] Di Ping, Gu Weisheng, Zhu Shigen. Effect of electrospark alloying process on microstructure and properties of the coating[J]. Journal of Dong Hua Univercity: English Edition, 2002, 22(4): 95-97.

[3] Wang a L, Fang a Y, Wu a P N, et al. Surface modification process by electrical discharge machining with a Ti powder green compact electrode[J]. Journal of Materials Processing Technology, 2002, 51(6): 139-142.

[4] Stachowiak G W, Batchelor A W. Surface hardening and deposition of coating on metal by a mobile source of localized electrical resistive heating[J]. Journal of Materials Processing Technology, 1996, 57(3): 288-297.

[5] 徐滨士, 朱绍华. 表面工程的基础理论[M]. 北京: 国防工业出版社, 1999.

作者简介: 张 平, 男, 1958年出生, 博士, 教授, 博士生导师. 主要从事焊接和材料表面改性的科研和教学工作. 发表论文 80余篇. Email: zhangp5801@sina.com

p 17—20

Abstract: To overcome the drawbacks of triditional structured-light sensor for field-teaching welding robot, off-line programming technique for virtual sensor is introduced. Firstly, the system architecture is designed, then the simulated sensor auto-modeling function is developped, the featured stripe profile for welding object is extracted based on the imaging principle of sensor in virtual scene, and at last actual featured profile recognition by using the programming result is discussed. Experiments on complex weld seam tracking and initial welding point search for strcutured component are executed, and results show the system can enhance the applicability and automation of structured-light sensors in robotic welding.

Key words: simulated sensors; structured-light vision; off-line programming; welding robot

Impact of external magnetic field generated by permanent magnet on quality of dual phase high strength steel by resistance spot welding

SHEN Qi, LI Yongbing, CHEN Guanlong, LIN Zhongqin (Shanghai Key Laboratory of Digital Autobody Engineering, Shanghai Jiaotong University, Shanghai 200240, China). p 21—24

Abstract: The joints of hot dip galvanized dual phase high strength steel (HDG-DP600) thick 2.25 mm were obtained by the resistance spot welding (RSW) process under the external constant magnetic field generated by a pair of hollow cylindrical permanent magnets, and the mechanical property, nugget size and grain structure of weld joints were analyzed. It was found that the tensile-shear force of the joints was increased by 11.01% compared with conventional RSW without the external constant magnetic field, the nugget diameter was increased by 5.20%; the crystal grain was refined and the nugget was' wide and flat. The result indicated that the external magnetic field generated by the permanent magnets can effectively improve the quality of the joints of RSW.

Key words: permanent magnet; dual phase high strength steel; resistance spot welding; mechanical property

Effect of Ag content on soldering ability of Sn-Ag-Cu solders

LIU Yang, SUN Fenglian, LIU Yang*, WANG Jiabing (College of Material Science and Engineering, Harbin University of Science and Technology, Harbin 150040, China). p 25—28

Abstract: The influences of Ag content on melting temperature and wettability of Sn-xAg-0.5Cu (x=0.3, 0.5, 0.7, 0.9) lead-free solder alloys were studied. The melting temperatures of alloys were compared by DSC (differential scanning calorimetry) curves and the wettability was compared by the area and rate of wetting on Cu substrate. The experimental results indicate that alloys with higher Ag content have lower melting points and melting range, and the content of Ag in solder alloys has a significant impact on the distribution and profile of the DSC curves. However, with the Ag content increasing, the wettability of the alloys degrades. By combining the two key properties of solder alloy, melting temperature and wettability, Sn-0.7Ag-0.5Cu shows higher performance.

Key words: lead-free solder; melting temperature; wettability

Analysis of stress corrosion cracking behavior of B101 coiled tubing

BI Zongyue[1,2], ZHANG Kun[1], LEI Ali[1], FENG Lajun[1] (1. School of Materials Science and Engineering, Xi'an University of Technology, Xi'an 710048, China; 2. Baoji Petroleum Steel Pipe Company Limited, Baoji 721008, China). p 29—32

Abstract: The behavior of H_2S stress corrosion cracking of coiled tubing was investigated, the fracture morphology was observed by scanning electron microscope, and the elemental composition of fracture was analyzed by energy disperse spectroscopy. The fracture mechanism was analyzed from the aspects of environment factor, material structure and chemical constitution. The results show that the base metal is insensitive to stress corrosion, and the weld is the weak region of stress corrosion. The weld fracture can be subdivided into four periods: crack incubation period, crack development period, crack rapid growth period with a smoother fractured surface and eventual failure period. The effect of stress change on sulfide stress corrosion cracking is relatively less in the yield strength of 72%—90%. The weld defect, segregation and inclusion are the main factors that make the coiled tubing have low resistance to hydrogen sulfide corrosion.

Key words: coiled tubing; H_2S; stress corrosion cracking

Technique of nickel-based alloy coating produced by hand electric-spark depositing process

ZHANG Ping[1], MA Lin[1,2], LIANG Zhijie[1], ZHANG Erliang[1] (1. Science and Technology Laboratory on Remanufacturing, Academy of Armored Force Engineering, Beijing 100072, China; 2. Office of Compliance Affair, Institute of Chemical Defense, Beijing 102205, China). p 33—36

Abstract: Because the surface properties of tool steel can be improved through nickel-base alloy coatings achieved by electric-spark deposition technology, the nickel-based strengthen alloy coating on the surface of steel 45 is achieved by the hand electric-spark deposition equipment. The effects of the processing parameters such as thickness, hardness and microdefect on the coatings are analyzed. Through some tests, the parameters are optimized and the coating with better properties is obtained. The study indicates that the coating with best combination property, which thickness is about 595 μm, microhardness is 362 HV and there are no apparent defects in the coating, is produced when the output voltage is 128 V, the output power is 1.2 kW, and the argon atmosphere is 5 L/min.

Key words: electric-spark deposition; nickel-based alloy; depositing technique

Comparative analysis for joint performance of duplex stainless steel by different arc welding methods

WANG Zhiyu, HAN Jian, SONG Hongmei, JIANG Laizhu, WU Weiwei, ZHANG Wei (Research and Development Center, Baoshan Iron & Steel Co., Ltd., Shanghai 201900, China). p 37—40

Abstract: The welding tests are conducted on 15 mm thick plates of duplex stainless steel 2205 by three different arc